

Supplementary Information

G-Factor and Well-Width Fluctuations as a Function of Carrier Density in the 2D Hole Accumulation Layer of Transfer Doped Diamond

*Golrokh Akhgar,^{*1} Lothar Ley,^{1,2} Daniel L. Creedon,³ Alastair Stacey,³ Jeffrey C. McCallum,³ Alex R. Hamilton⁴ and Christopher I. Pakes^{§1}*

¹ Department of Chemistry and Physics, La Trobe University, Victoria 3086, Australia

² Institute of Condensed Matter Physics, Universität Erlangen, Staudt-Str. 1, 91058 Erlangen, Germany

³ School of Physics, The University of Melbourne, Victoria 3010, Australia

⁴ School of Physics, University of New South Wales, Sydney, New South Wales 2052, Australia

I. Determining the hole-hole interaction correction

In 2D samples quantum corrections are due to the Weak Localisation and Weak Anti localisation and Hole-hole interaction (HHI). The conductivity corrections due to $\Delta\sigma_{WL}$, $\Delta\sigma_{WAL}$ and $\Delta\sigma_{HHI}$ to the longitudinal conductivity is given by the equation below while Hall conductivity is not affected:

$$\Delta\sigma_{xx} = \Delta\sigma_{WL} + \Delta\sigma_{WAL} + \Delta\sigma_{HHI} \quad (S1)$$

Starting with HHI correction; this intrinsic quantum correction to the resistivity does not connected to the phase coherent backscattering of electrons/holes (WL and WAL). The main comparison to magnetoconductivity effects is that HHI is independent of magnetic field and

it is the interaction of two different holes instead of interaction of a hole to itself. The theoretical framework of HHI is developed by Alshuler and Aronov [1] and it is originally based on electron systems, but similar approach can be used for p-type samples. We adopt method II by Goh et al. [2] to extract hole-hole interaction strength, K_{hh} . This is done by subtraction HHI correction term $\Delta\sigma_{HHI}$ to the longitudinal conductivity from both ρ_{xx} (B) and ρ_{xy} (B) traces. This method of HHI correction is previously applied and described on H-terminated diamond devices [3]. The HHI correction term to the Drude conductivity is given by:

$$\Delta\sigma_{HHI} = K_{hh}G_0\ln\left(\frac{k_bT\tau}{\hbar}\right) \quad (S2)$$

Where $G_0 = e^2/\pi\hbar$, T is the temperature, K_{hh} is the dimensionless Coulomb interaction strength, and $\tau = \sigma_D m^*/pe^2$ is the transport relaxation time with p the areal hole density, σ_D the Drude conductivity and m^* the effective hole mass for dispersion in the plane of the 2D system. We adopt the value $m^* = 0.208m_0$ for the 2D heavy hole mass, [4] and equate σ_D to $\sigma_{xx}(30\text{ K})$ to obtain τ from the longitudinal conductivity. The values of σ_D and τ for different gate voltages are listed in Table SI.

Figure S1 shows logarithmic dependence of the HHI correction. The K_{hh} is determined by slope of ΔR_H Vs $\ln(T)$:

$$K_{hh} = -\frac{\text{Hall slope} \times \sigma_{xx}(30\text{ K})}{2G_0} \quad (S3)$$

where $\Delta R_H(T) = (R_H(T) - R_H(20\text{ K}))/R_H(20\text{ K})$ under assumption that Hall resistivity at 20 K approaches its Drude limit.

K_{hh} are determined for each gate bias via the following process and listed in Table S1. Once τ and K_{hh} are evaluated, the B independent $\Delta\sigma_{HHI}$ is calculated from equation (S1) for all temperatures at each gate voltage. Then the corrected conductivity without HHI, $\sigma_{xx}(B, T, V_g)$,

is calculated by subtracting the $\Delta\sigma_{HHI}(B, T, V_g)$ from the original $\sigma_{xx}^{Measured}(B, T, V_g) \approx 1/\rho_{xx}^{Measured}(B, T, V_g)$ (in the limit $\rho_{xy} \ll \rho_{xx}$ which holds in all cases here). After subtraction, a corrected $\rho_{xy}(B, T, V_g) = \frac{\sigma_{xy}^{Measured}}{\sigma_{xx}^{Corrected}}$, is also calculated. After subtraction of HHI from $\rho_{xx}(B)$ and $\rho_{xy}(B)$, the corrected $\rho_{xy}(B, T, V_g)$ traces should collapse onto one single trace, otherwise, K_{hh} should be systematically adjusted and $\Delta\sigma_{HHI}$ should be recalculated until all $\rho_{xy}(B)$ traces collapse onto one curve as it shows in Figure S2 [3]. The corresponding adjusted K_{hh} are listed in Table S1 for all gate biases. When the final K_{hh} is established for all gate voltages, a similar K_{hh} is used for HHI correction in each set of measurements with constant in-plane magnetic field. The remaining parameters in Table S1 are the hole mean free path, $l = ((2\pi)^{1/2}\hbar\sigma_D)/(e^2p^{1/2})$, the diffusion constant, $D = l^2/(2\tau)$, and the transport magnetic field, $B_{tr} = \hbar/(2el^2)$.

Figure S3 shows the corresponding magneto-resistivity data before (solid lines) and after (dashed lines) HHI removal.

II. Fitting magnetoconductivity data to 2D localisation theory

The dominant spin-orbit interaction mechanism is k^3 Rashba-like mechanism [5]. The corrected magnetoconductivity data $\Delta\sigma$ for different temperatures are plotted in Figure S4 and fitted to the k^3 Rashba using eq. S4. The spin and phase characteristic fields B_{so} and B_ϕ are extracted for each gate bias from the fits. Phase and spin coherence lengths are calculated using $L_\phi = (\hbar/(4eB_\phi))^{0.5}$ and $L_{so} = (\hbar/(4eB_{so}))^{0.5}$ respectively and plotted in Figure S5 for all gate biases. The scale $L_\phi \sim T^{-0.5}$, confirms the two dimensionality of this system. The variation of L_{so} with hole density is plotted in Figure S6(b).

$$\Delta\sigma = \frac{e^2}{2\pi^2\hbar} \left[\Psi\left(\frac{1}{2} + \frac{B_\phi + B_{so}}{B}\right) + \frac{1}{2}\Psi\left(\frac{1}{2} + \frac{B_\phi + 2B_{so}}{B}\right) - \frac{1}{2}\Psi\left(\frac{1}{2} + \frac{B_\phi}{B}\right) - \ln\left(\frac{B_\phi + B_{so}}{B}\right) - \frac{1}{2}\ln\left(\frac{B_\phi + 2B_{so}}{B}\right) + \frac{1}{2}\ln\left(\frac{B_\phi}{B}\right) \right] \quad (S4)$$

After fitting the magnetotransport data, the phase relaxation time $\tau_\phi = \hbar/(4eDB_\phi)$ calculated and plotted in Figure S6(c), it shows no dependency in gate bias and scales as $\tau_\phi \sim T^{-1}$, showing the evidence for a scattering mechanism consistent with Nyquist dephasing as expected in a weakly disordered 2D system [2, 6]. The spin orbit interaction is calculated from $\Delta_{SO} = \hbar/(2\tau\tau_{SO})^{1/2}$ where $\tau_{SO} = \hbar/(4eDB_{SO})$ is the spin relaxation time. Δ_{SO} is plotted as a function of density in Figure S6 (d).

III. Fitting magnetoconductivity data in the presence of an in-plane magnetic field

We performed magnetotransport measurements in the presence of constant B field. Constant in-plane B field, $B_{||}$, in the range of 0 to 1 T with steps of 0.2T is applied while sweeping the perpendicular magnetic field from -1 to 1T. The B_ϕ and B_{SO} remains constant as a function of $B_{||}$ for that reason we use the same B_{SO} and B_ϕ that we extract from the equation above at 2.5K. and by following Minkov *et. al.* method [7] Zeeman splitting and interface roughness terms are extracted. This is done by adding Zeeman term to singlet terms of the equation S4 and interface roughness to both singlets and triplets:

$$\Delta\sigma = \frac{e^2}{2\pi^2\hbar} \left[\Psi\left(\frac{1}{2} + \frac{B_\phi + B_{SO} + \Delta_r}{B}\right) + \frac{1}{2}\Psi\left(\frac{1}{2} + \frac{B_\phi + 2B_{SO} + \Delta_r}{B}\right) - \frac{1}{2}\Psi\left(\frac{1}{2} + \frac{B_\phi + \Delta_S + \Delta_r}{B}\right) - \ln\left(\frac{B_\phi + B_{SO} + \Delta_r}{B}\right) - \frac{1}{2}\ln\left(\frac{B_\phi + 2B_{SO} + \Delta_r}{B}\right) + \frac{1}{2}\ln\left(\frac{B_\phi + \Delta_S + \Delta_r}{B}\right) \right] \quad (S5)$$

Δ_S and Δ_r is extracted for each gate bias and plotted as a function of $B_{||}^2$.

IV. Calculation of hole band dispersion

The 2D dispersion curves of the heavy hole and light hole bands, calculated using the approach of ref [8] with a triangular well approximation, are given in Figure S7. The energy dispersion, $E = \hbar^2 k^2 / (2m_0 m_{eff})$, where we have adopted the effective mass values of $m_{hh}^* = 0.208m_0$ and $m_{lh}^* = 0.288m_0$ for the heavy hole and light hole respectively from Ref [4, 9] that are appropriate for the direction parallel to the surface of diamond.

References:

1. Altshuler, B.L. and A.G. Aronov, *Electron–electron interaction in disordered conductors*, in *Modern Problems in condensed matter sciences*. 1985, Elsevier. p. 1-153.
2. Goh, K., M. Simmons, and A. Hamilton, *Electron-electron interactions in highly disordered two-dimensional systems*. *Physical Review B*, 2008. **77**(23): p. 235410.
3. Akhgar, G., et al., *Strong and Tunable Spin–Orbit Coupling in a Two-Dimensional Hole Gas in Ionic-Liquid Gated Diamond Devices*. *Nano letters*, 2016. **16**(6): p. 3768-3773.
4. Edmonds, M.T., et al., *Spin–Orbit Interaction in a Two-Dimensional Hole Gas at the Surface of Hydrogenated Diamond*. *Nano letters*, 2014. **15**(1): p. 16-20.
5. Knap, W., et al., *Weak antilocalization and spin precession in quantum wells*. *Physical Review B*, 1996. **53**(7): p. 3912.
6. Altshuler, B.L., A. Aronov, and D. Khmelnitsky, *Effects of electron-electron collisions with small energy transfers on quantum localisation*. *Journal of Physics C: Solid State Physics*, 1982. **15**(36): p. 7367.
7. Minkov, G., et al., *Weak antilocalization in quantum wells in tilted magnetic fields*. *Physical Review B*, 2004. **70**(15): p. 155323.
8. Ando, T., A.B. Fowler, and F. Stern, *Electronic properties of two-dimensional systems*. *Reviews of Modern Physics*, 1982. **54**(2): p. 437.
9. Naka, N., et al., *Direct measurement via cyclotron resonance of the carrier effective masses in pristine diamond*. *Physical Review B*, 2013. **88**(3): p. 035205.

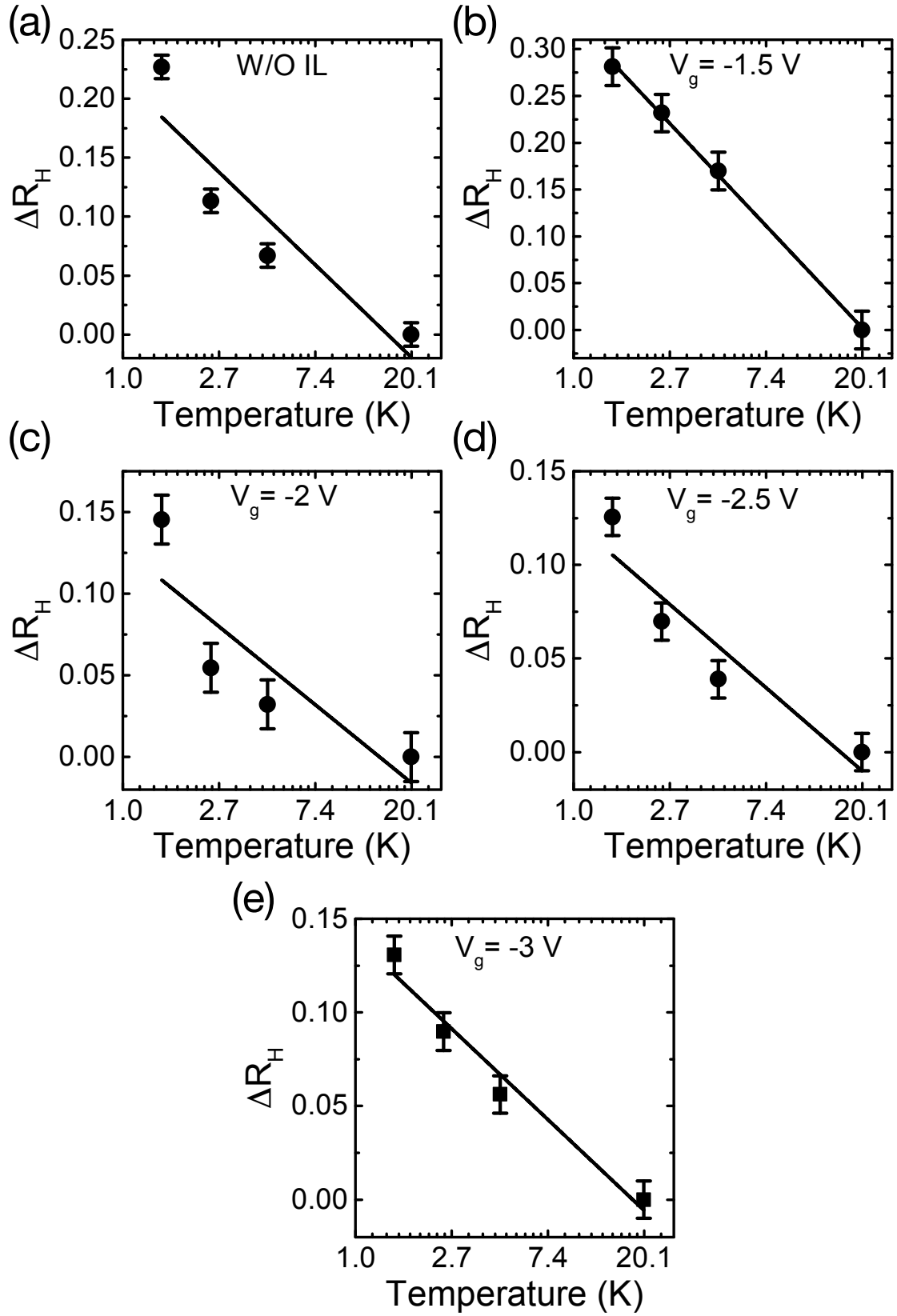


Figure S1: ΔR_H plotted as a function of temperature for all different gate biases. Demonstrating logarithmic dependence on T . The slope of these plots are used to calculate the value of K_{hh} as explained in the text.

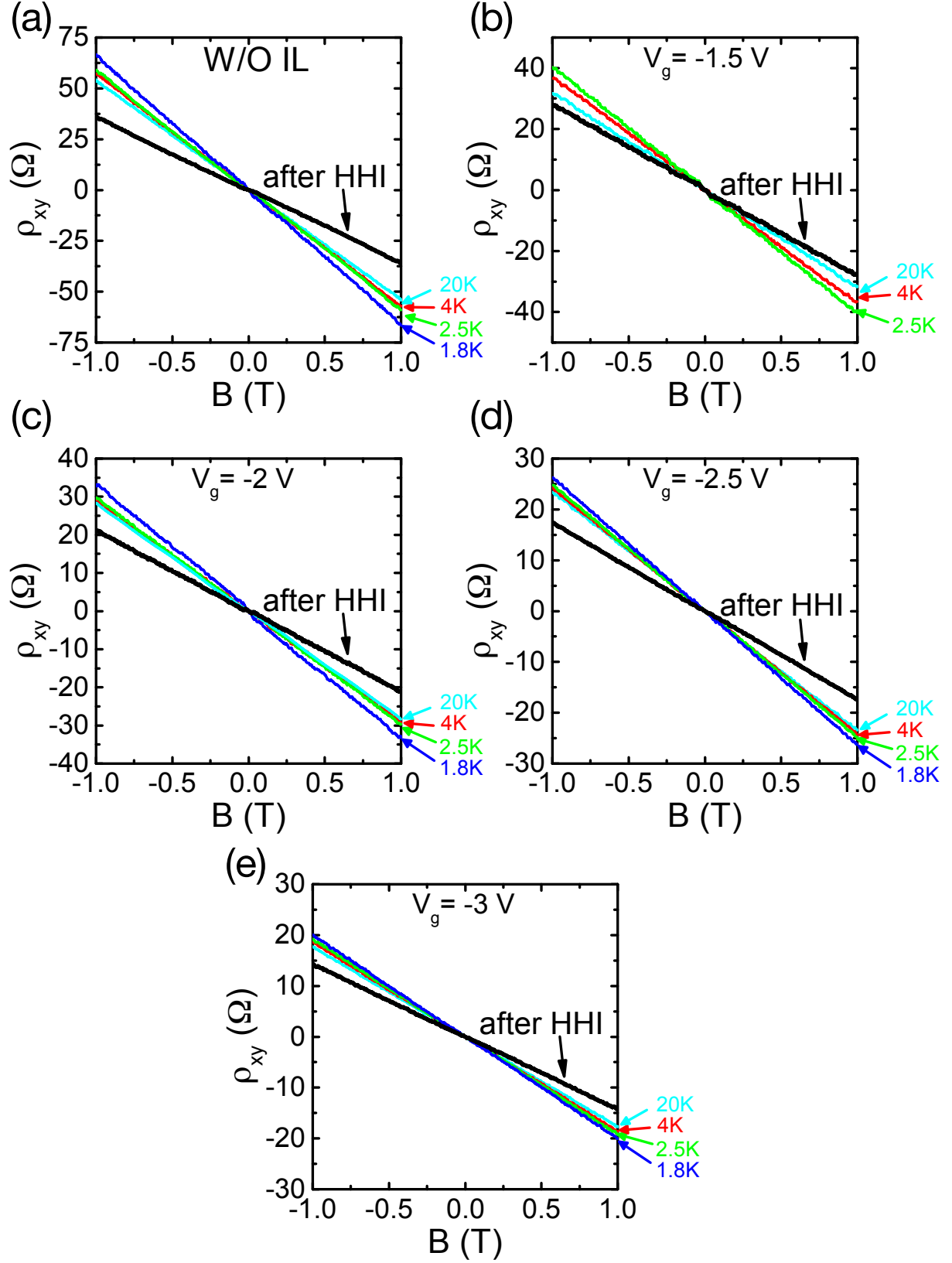


Figure S2: $\rho_{xy}(B)$ before and after HHI removal. Corrected traces of all temperatures are collapsed onto one trace after successful removal of $\Delta\sigma_{HHI}$ from the measured magnetotransport data.

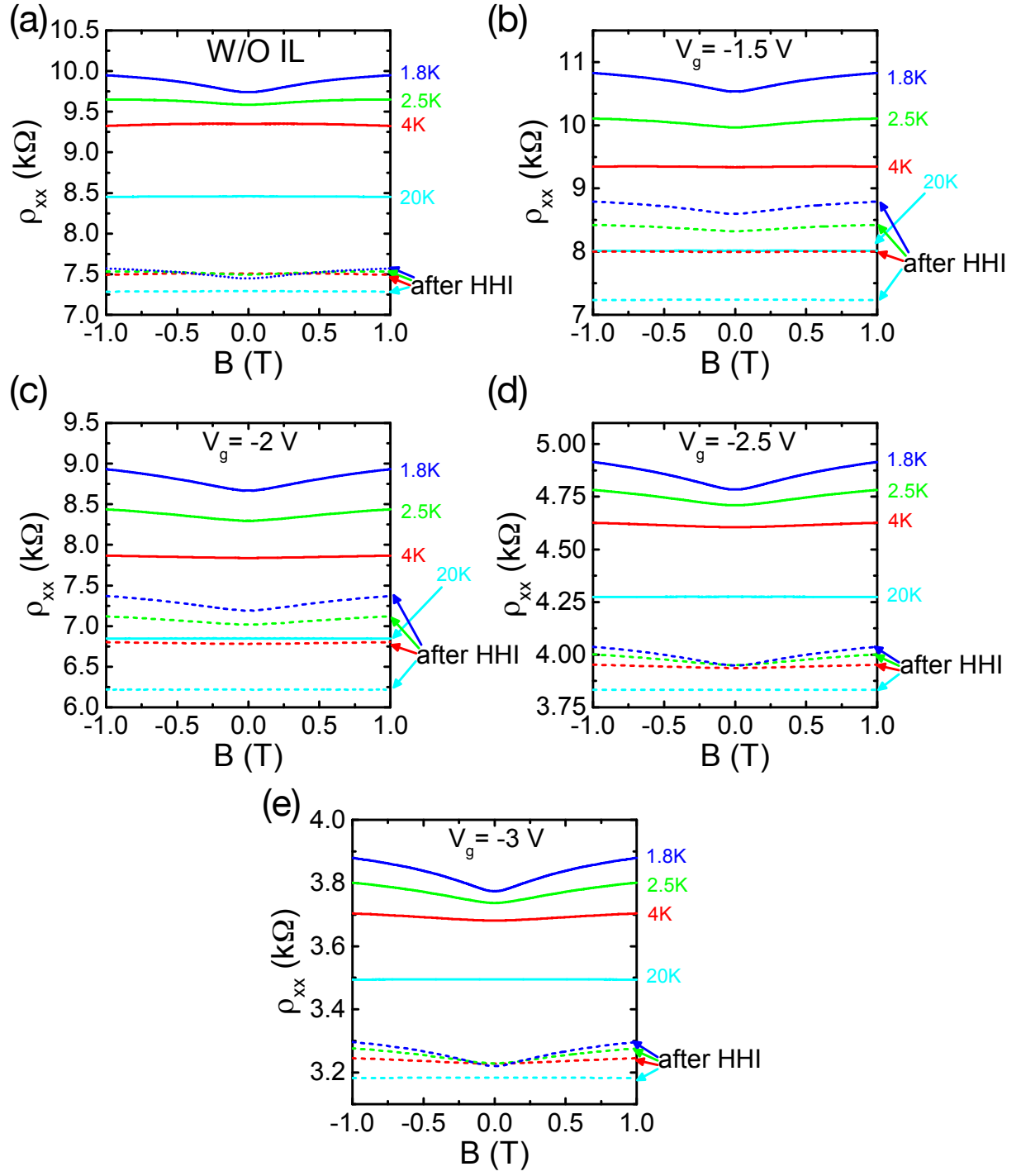


Figure S3: $\rho_{xx}(B)$ before and after successful removal of $\Delta\sigma_{HHI}$ from the measured magnetotransport data.

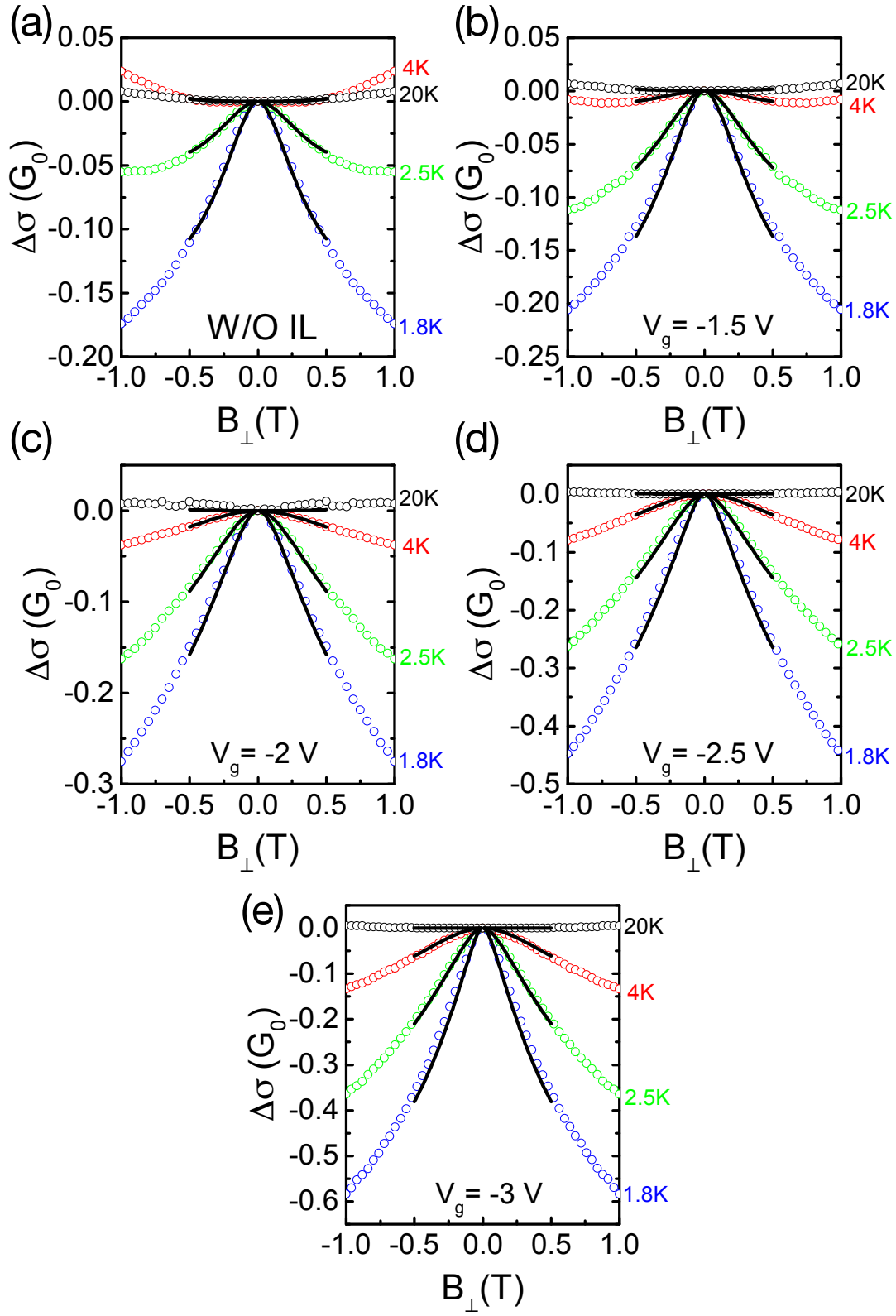


Figure S4: Reduced magnetoconductivity (in units of $G_0 = e^2/\pi h$), at different temperatures plotted for all gate voltages. The black solid lines correspond to fits to equation 4.

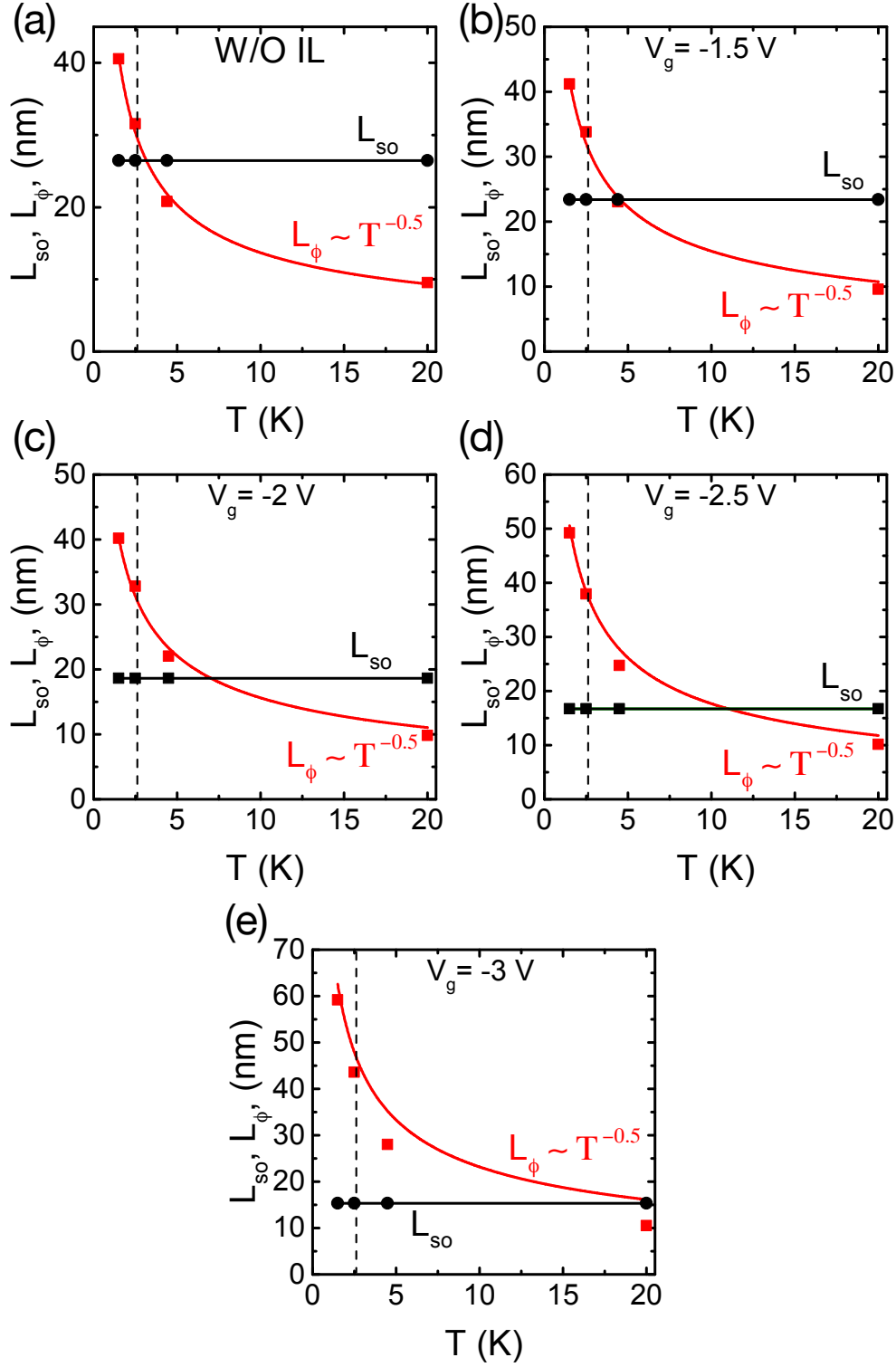


Figure S5: Temperature dependence of the characteristic spin coherence lengths, L_{SO} , (black circle) and phase coherence lengths, L_{ϕ} , (red square) with gate voltage V_g as parameter. The lines represent a $T^{-0.5}$ fit for L_{ϕ} .

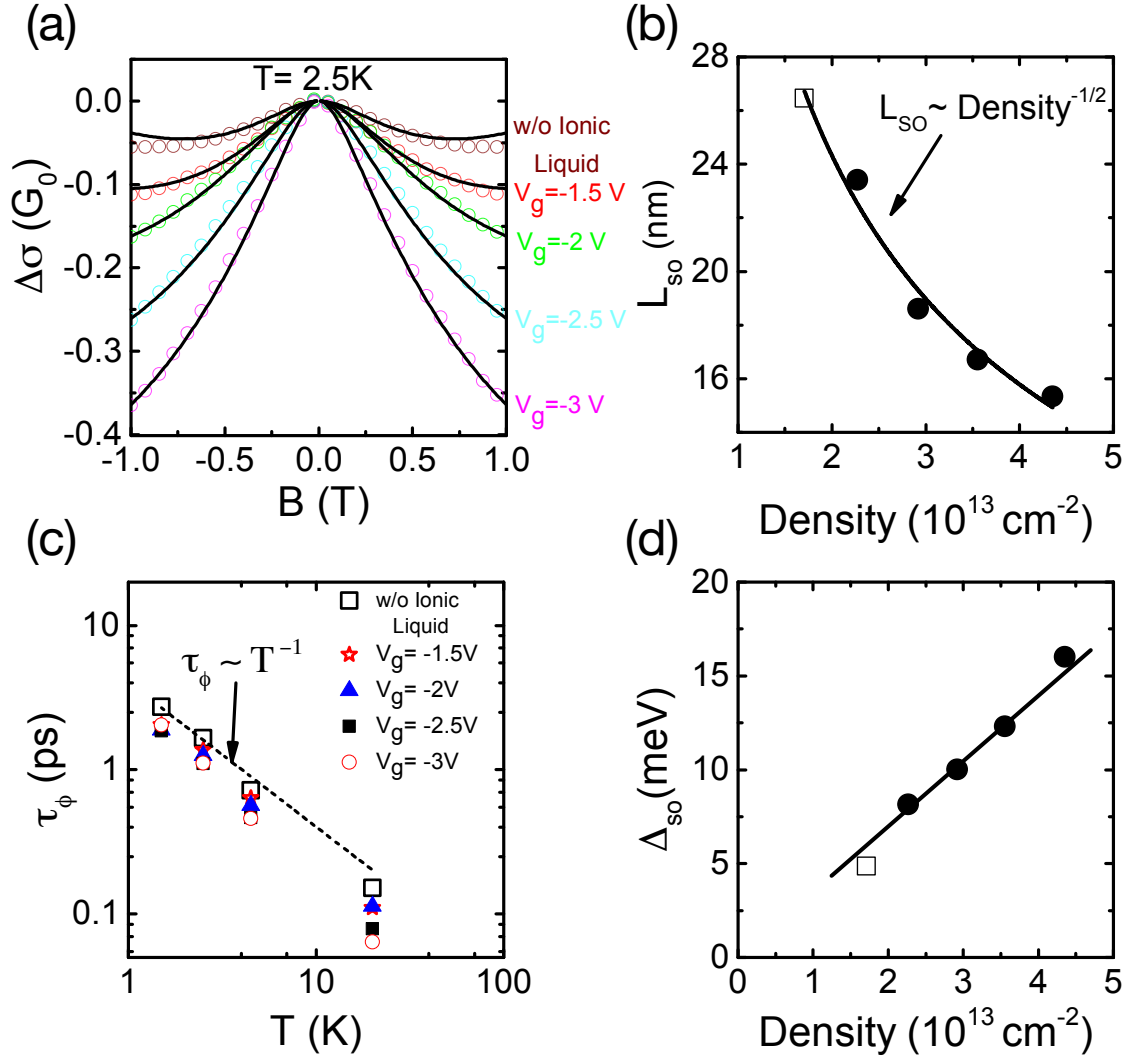


Figure S6: (a) Reduced magnetoconductivity, $\Delta\sigma = \sigma(B) - \sigma(B = 0)$ (in units of $G_0 = e^2/\pi h$), for different gate bias at 2.5 K; (b) spin coherence length L_{so} as a function of hole density; (c) temperature dependence of the dephasing time (τ_ϕ) plotted at different gate biases; the broken line indicates $\tau_\phi \sim T^{-1}$ consistent with Nyquist dephasing; (d) tuning of the spin-orbit splitting strength, Δ_{so} , with hole sheet density; the solid line is a linear fit to the data. The open squares represent the data obtained for the un-gated device in all figures.

Table S1: Summary of calculated parameters

Gate Voltage, V_g [V]	w/o IL	-1.5	-2.0	-2.5	-3.0
Estimated Interaction strength, K_{hh} , obtained from the slope of normalised $\rho_{xy}/B(\Omega/T)$ vs. $\ln(T)$	0.396	0.554	0.309	0.436	0.578
Interaction strength, K_{hh} , obtained from collapsing all $\rho_{xy}^{Measured}(B)$ onto one curve ($\rho_{xy}^{Corrected}(B)$)	0.40±0.01	0.25±0.03	0.28±0.03	0.54±0.01	0.55±0.01
Hole sheet density, p , before HHI removal [$10^{13}cm^{-2}$] (20K)	1.16	1.98	2.19	2.67	3.52
Hole sheet density, p , after HHI removal [$10^{13}cm^{-2}$]	1.17	2.27	2.92	3.55	4.35
Drude conductivity, σ_D [$10^{-4}\Omega^{-1}$] (30K)	1.23	1.33	1.58	2.42	2.94
Transport relaxation time, τ [fs]	7.9	4.95	4.33	6.68	6.15
Mean free path, l [nm]	3.1±0.1	2.9±0.1	3.0±0.2	4.2±0.5	4.6±0.5
Diffusion coefficient, D [$10^{-3}m^2s^{-1}$]	0.9±0.1	1.0±0.1	1.1±0.1	1.7±0.2	2.1±0.2
Characteristic transport field, B_{tr} [T]	34.52	39.88	36.01	18.86	15.62

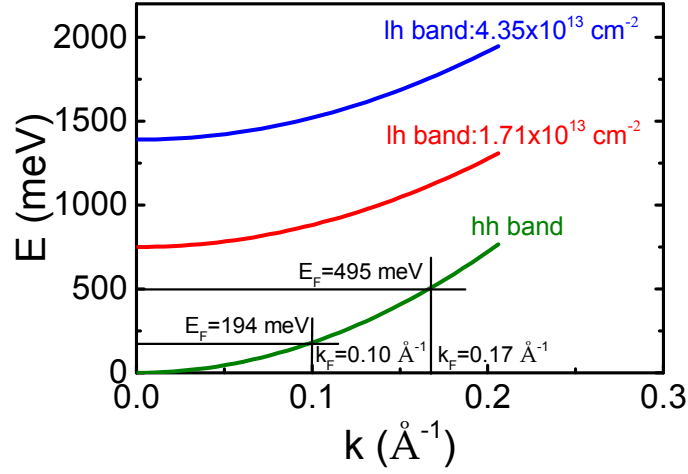


Figure S7: shows the 2D hole dispersion for lowest and highest density achieved in this experiment for k in the (100) plane. $k_F = (2\pi p)^{1/2}$ is the Fermi wave vector where p the areal hole concentration, and $E_F = pe/\epsilon_0\epsilon_D$ is the Fermi energy where ϵ_0 is the permittivity of vacuum and $\epsilon_D = 5.7$ is the permittivity of diamond.